AIMS Geosciences, 11(4): 867–884.
DOI: 10.3934/geosci.2025037
Received: 26 March 2025
Revised: 15 May 2025
Accepted: 04 June 2025
Published: 22 October 2025

https://www.aimspress.com/journal/geosciences

Research article

Numerical investigation of the diversion length for the capillary barrier system

Shijun Wang[1], Yunfei Tian[1], Jing Yang[1], Huihui Xu[1], Hailong Zhang[1], Xianting Yi[2] and Qian Zhai[2,3,*]

[1] Gansu Electric Power Corporation, State Grid Corporation of China, Lanzhou, 730050, China
[2] School of Civil Engineering, Southeast University, Jiangsu Nanjing 211189, China
[3] Advanced Ocean institute of Southeast University, Southeast University，Jiangsu Nantong 226010, China

*** Corresponding:** Email: zhaiqian@seu.edu.cn.

Abstract: The capillary barrier system (CBS) is commonly used to control rainwater infiltration into the slope soil and enhance slope stability under rainfall conditions. In the CBS, a fine-grained layer is commonly overlayered on top of the coarse-grained layer. Because the hydraulic conductivity of unsaturated coarse-grained soil is much lower than that of fine-grained soil, the infiltrated rainwater flows only in the fine-grained layer. With the accumulation of the rainwater, rainwater in the fine-grained layer can finally penetrate the coarse-grained layer, and "breakthrough" occurs. The horizontal length from the initial point to the breakthrough point is commonly defined as the diversion length (L). Various empirical models have been proposed for the estimation of L, but the results from those empirical equations differ from each other. In this paper, the limitations associated with different empirical models for the estimation of L were discussed. Subsequently, both diversion lengths and the time corresponding to the breakthrough obtained from numerical analyses were presented and compared with those from empirical equations. When the rainfall intensity is higher than 10% of k_s of fine-grained soil, the empirical models showed that L increases with the increase in slope angle, while the numerical results showed the opposite. Empirical models were based on steady-state infiltration analysis, while the numerical models were based on transient infiltration analysis. The results in this paper indicate that the numerical results are more reliable than those from empirical equations.

Keywords: capillary barrier system (CBS); diversion length (*L*); numerical analysis; steady-state infiltration; transient infiltration

1. Introduction

Fourie [1] indicated that rainfall-induced slope failures were a major pattern of slope failures in the tropical area. The works from Rahardjo et al. [2], Rahardjo et al. [3], and Zhai et al. [4] indicated that rainwater infiltration was the triggering factor leading to slope failure under rainfall. Rahardjo et al. [2] and Zhang et al. [5] suggested that controlling rainwater infiltration was the optimal method to prevent rainfall-induced slope failure. The capillary barrier system (CBS) was proposed by Nicholson et al. [6], Stormont and Morris [7], and Rahardjo et al. [8], and consists of overlaying a fine-grained layer on top of a coarse-grained layer to control rainwater infiltration into the slope soil. Zhai et al. [9–11] demonstrated that the hydraulic conductivity of coarse-grained soil was much lower than that of fine-grained soil when the soils are in unsaturated conditions. Ross [12] indicated that water in the fine-grained layer could penetrate the coarse-grained layer with the accumulation of pore-water pressure in fine-grained soil. If the accumulated water exceeded the diversion capacity of the CBS, water in the fine-grained layer would penetrate the coarse-grained layer; the point at which such penetration occurs is commonly referred to as the "breakthrough" point. The maximum horizontal distance from the initial point to the breakthrough point is commonly defined as the diversion length (*L*). The value of *L* is crucial for the evaluation of the performance of the CBS and a controlling index for the design of the CBS surface drain.

Stormont [13] conducted a series of experiments to investigate the performance of CBS on a 10° slope under two scenarios: (i) no discharging drain installed, and (ii) discharging drains installed at 10 m intervals. The same rainfall condition, with intensity (*q*) of 10 mm/day, was applied in both designs. It was observed that there was no rainwater penetrating the CBS in design (ii), while a breakthrough was observed in design (i). The experimental results from Stormont [13] indicated that the discharging drain was important for the CBS design, and *L* was a key parameter for the design of the discharging drain. Therefore, the determination of *L* is crucial for the design of CBS.

Ng et al. [14] conducted a physical model of a three-layer CBS (silt/gravelly sand/clay) with a slope angle of 10°. They observed no breakthrough on the silt–gravelly sand interface in the first 1.5 h, while the same changed from 1.2 kPa at 1.5 h to 0 kPa at 4 h in gravelly sand. The results indicate that the breakthrough occurred on the silt–gravelly sand interface between 1.5 and 4 h. On the other hand, Chen et al. [15] measured the surface run-off of the three-layer CBS (silt/gravelly sand/clay) with slope angles of 3°, 10°, and 18°. They observed that the surface runoff for the model with a slope angle of 3° was higher than that of 10° and 18°. Therefore, slope angle plays an important role on the actual infiltration rate into sloped soil.

In this paper, the empirical equations for the determination of *L* are reviewed, and the limitations associated with those empirical equations are discussed. Subsequently, transient infiltration analyses are conducted to compute the *L* of CBS for different scenarios. The results from the numerical analyses indicate that the time to breakthrough is a function of the thickness of the fine-grained layer, regardless of slope angle.

2. Empirical models for the estimation of *L*

In this section, *L* is first defined; subsequently, the empirical models for the estimation of *L* are reviewed and discussed. The limitations associated with those empirical models are also explained in this section.

2.1. Definition of L

Hill and Parlange [16] and Stormont and Anderson [17] indicated that the difference between the hydraulic conductivities of soils in fine-and coarse-grained layers was the governing parameter for the design of CBS. During rainfall, infiltrated water cannot infiltrate further into the coarse-grained layer because its hydraulic conductivity is much lower than that of fine-grained soil. However, if the water in the fine-grained layer cannot drain in time, water would accumulate there, which in turn would result in a high hydraulic gradient on the interface of fine- and coarse-grained layers. As a result, rainwater would finally penetrate the coarse-grained layer, spoiling the capillary barrier and allowing breakthrough to occur.

Shackelford et al. [18] and Stormont [19] defined the horizontal distance between the initial point and the breakthrough point to be the diversion length, as illustrated in Figure 1. The lateral distance from the initial point and the breakthrough point is commonly referred to as the lateral diversion length. Yang et al. [20] and Kung [21] indicated that *L* depends on factors such as the hydraulic properties of both fine- and coarse-grained soils, the thickness of the fine-grained layer, the infiltration rate, the existing ground water table (GWT), and the slope angle. Zhai et al. [22,23] indicated that both soil–water characteristic curve (SWCC) and the hydraulic conductivity function (HCF) were major hydraulic properties governing the infiltration rate into the surface soil. Therefore, both the SWCCs and HCFs of fine- and coarse-grained soils were essential information required for the evaluation of the *L* in the design of CBS.

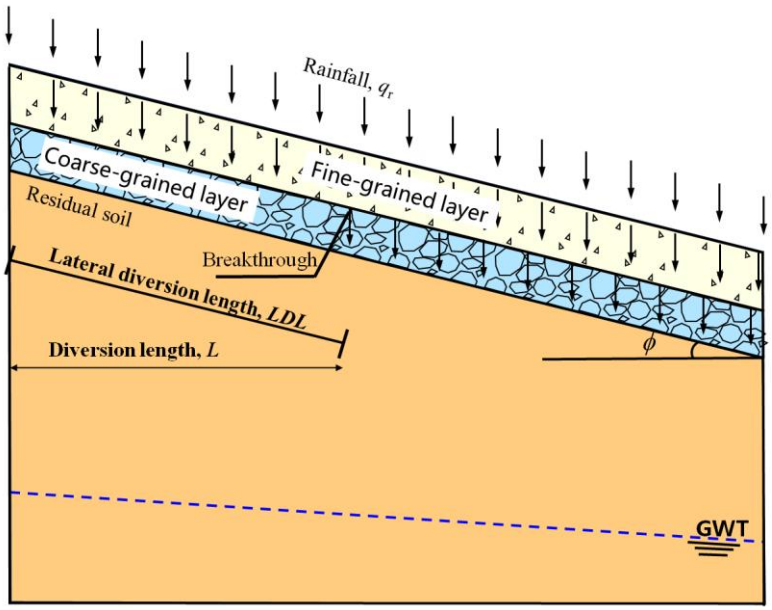

Figure 1. The illustration of *L* (modified from Stormont [19]).

2.2. Mathematical models for the estimation of L

Ross [12] adopted the steady-state infiltration analysis, as shown in Figure 2, and proposed an empirical model for the estimation of the L from the HCF of the fine-grained soil and the infiltration rate (q), as illustrated in Equation (1). Ross's equation [12] was considered to be the first attempt at the estimation of the diversion length of CBS.

$$L = \frac{k_s \tan\phi \int_{\psi_i}^{0} k_r(\psi) d\psi}{q} \tag{1}$$

where L is the length of CBS, k_s is the saturated hydraulic conductivity of fine-grained soil, $k_r(\psi)$ is the relative hydraulic conductivity corresponding to the soil suction of ψ, which can be defined as $k_r(\psi)=k_{unsat}/k_s$, k_{unsat} is the hydraulic conductivity of unsaturated fine-grained soil, ψ is the soil suction, ψ_i is the initial soil suction in the fine-grained soil, ϕ is the slope angle, and q is the infiltration rate.

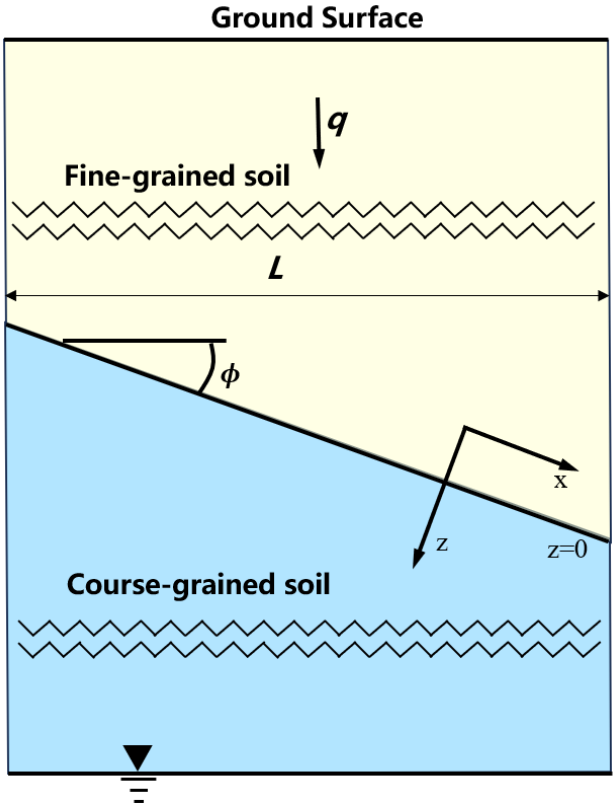

Figure 2. Schematic diagram of the model from Ross [12].

As illustrated in Figure 2, Ross [12] adopted the infiltration rate (q) rather than rainfall intensity to estimate the diversion length of CBS. In addition, the groundwater table (GWT) was assumed to be far away from the interface of fine-grained and coarse-grained layers. In addition, Ross [12] adopted 1D infiltration to estimate the suction profile in the fine-grained layer. Ross [12] defined that the breakthrough occurred when the infiltration rate was higher than the discharging rate, as shown in Figure 3.

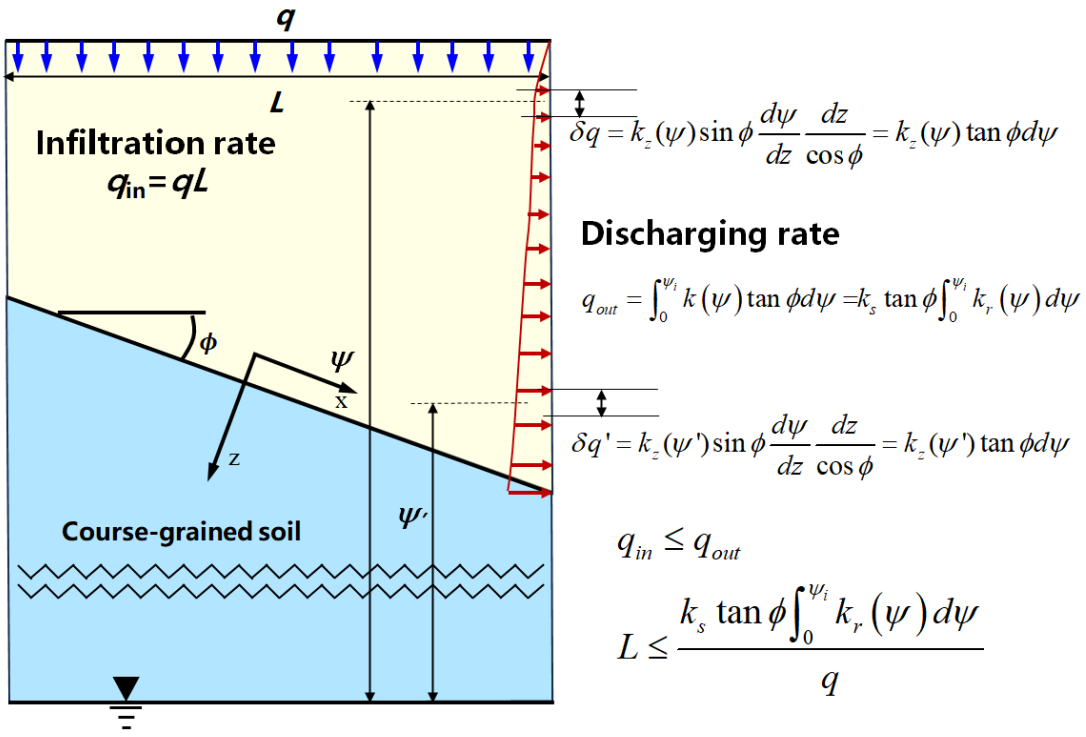

Figure 3. Illustration of the estimation of diversion length of CBS from Ross's method [12].

As illustrated in Figure 3, the suction profile in the fine-grained layer was assumed to be proportional to its elevation (*z*), based on the assumption of the steady-state infiltration analysis. As shown in Equation (1), the diversion length (*L*) of the CBS was only governed by the hydraulic property of fine-grained soil and did not depend on the hydraulic properties of coarse-grained soil. If the hydraulic properties of coarse-grained soil are close to those of fine-grained soil, then there is no capillary barrier effect. Therefore, the hydraulic conductivity of the coarse-grained soil should be considered in the determination of *L*. The suction profile was determined using Darcy's law, where the one-dimensional steady-state infiltration could be expressed as follows:

$$-q = k(\psi)\left(\frac{\partial\psi}{\partial z} - 1\right) \tag{2}$$

where *q* is the infiltration rate, k(ψ) is the unsaturated hydraulic conductivity of soil at a suction level of ψ, ψ is the capillary tension, and *z* is the altitude. As shown in Equation (2), the infiltration rate is independent of time.

Steenhuis et al. [24] adopted Rijtema's (1965) model, as shown in Equation (2), to represent the hydraulic conductivity of the fine-grained soil and proposed another model for the estimation of *L* by modifying Ross's model [12]. Steenhuis et al. [24] considered that when the soil suction in the fine-grained layer reached the water-entry value (WEV) of the coarse-grained soil, rainwater in the fine-grained layer would penetrate the coarse-grained layer. Therefore, the minimum suction value in Equation (1) was limited by the WEV of the coarse-grained soil rather than zero.

$$\begin{cases} k = k_{sat} & \psi \le \text{AEV} \\ k = k_{sat} e^{-\alpha(\psi - AEV)} & \psi > \text{AEV} \end{cases} \tag{3}$$

where AEV is the air-entry value, α is the model parameter, and ψ is the soil suction.

$$L = \frac{k_s \tan\phi \left[\alpha^{-1} + \left(AEV_f - WEV_c \right) \right]}{q} \tag{4}$$

where AEV_f is the air-entry value of the fine-grained soil, and WAV_c is the water entry value of coarse-grained soil.

Both Ross [12] and Steenhuis et al. [24] adopted the drying HCF of the fine-grained soil for the estimation of the diversion length of CBS. It should be noted that the infiltration process is a wetting process rather than a drying process, and the wetting HCF of the fine-grained soil should be used for the estimation of *L*.

Parent and Cabral [25] defined the suction corresponding to the hydraulic conductivity of the coarse-grained soil, equal to the infiltration rate (*q*), as ψ_{c_Coarse}, and the suction corresponding to the hydraulic conductivity of the fine-grained soil, equal to the infiltration rate (*q*), as ψ_{c_Fine}, as illustrated in Figure 4. Parent and Cabral [25] adopted ψ_{c_Coarse} as the minimum suction and ψ_{c_Fine} as the maximum suction in the fine-grained layer, improving Ross [12]'s model. Based on numerical analyses, Parent and Cabral [25] suggested a modification of the infiltration rate in Equation (1), as illustrated in Equation (5).

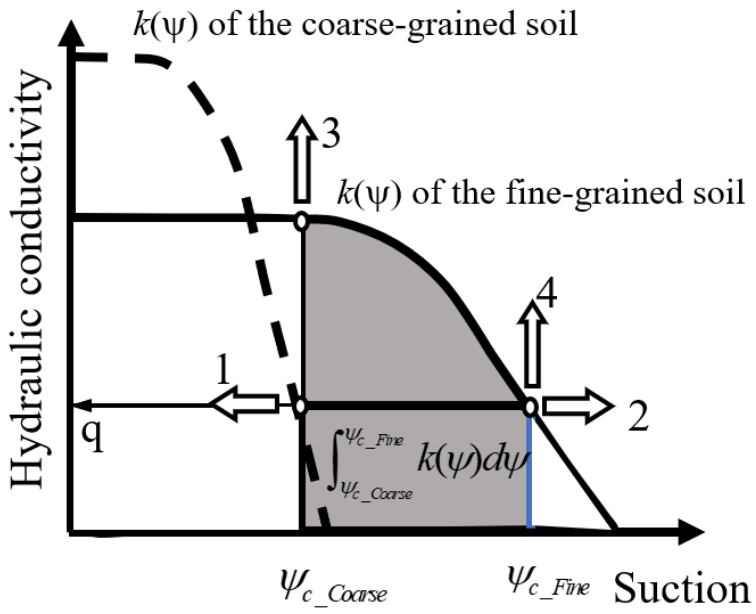

Figure 4. Illustration of ψ_{c_Coarse} and ψ_{c_Fine} in the fine-grained layer from Parent and Cabral [25].

$$L = \frac{k_s \tan\phi \int_{\psi\_Coarse}^{\psi\_Fine} k_r(\psi)d\psi}{0.998q^{1.024}} \tag{5}$$

On the other hand, Kung [21] adopted the theory of the funnel mechanism and proposed Equation (6) to estimate L. It should be noted that Kung's model [21] was also based on the steady-state infiltration analysis.

$$L = \frac{k_s AEV_f \sin\phi}{q\rho g} \tag{6}$$

Where AEV_f is the air-entry value of the fine-grained soil, ρ is the density of water, and g is the gravitational acceleration.

Stormont [13], Yang et al. [20], and Liu et al. [26] indicated that those empirical equations provided convenience to geotechnical engineers to estimate the diversion length of CBS. It should be noted that existing models were proposed based on the assumption that the infiltration rate was much less than the k_s of fine-grained soil. However, the works by Rahimi et al. [27], Liu et al. [28], Cuomo et al. [29], and Liu et al. [30] indicated that when rainfall intensity was close to the k_s of surface soil, some rainwater would be discharged in the form of run-off. As a result, the limitations associated with those models could be summarized as follows: (1) The transient infiltration analysis should be used rather than the steady-state infiltration analysis; (2) the infiltration is the wetting process, and wetting HCF rather than the drying HCF should be used; (3) those empirical equations may not be applicable for the case when rainfall intensity is close to the k_s of fine-grained soil; and (4) the criteria for the determination of the breakthrough condition is unclear.

In this paper, a series of transient infiltration analyses was conducted by using the commercial software GeoStudio (Seep/W). The effects of factors such as the thickness of the fine-grained layer, slope angle, and rainfall intensity on the determination of diversion length were investigated. In addition, the times corresponding to the breakthrough condition for different cases were also investigated and discussed.

3. Numerical analyses

To investigate the diversion length, a typical slope was used for the transient seepage analyses. The hydraulic boundary conditions are illustrated in Figure 5. To eliminate the effect of the existing slope soil on the performance of CBS, the existing slope soil was not modeled in the study. The drainage boundary condition was assigned to AK, KJ, BC, and CD, the total Q equal to 0 was assigned to JD, and the rainfall boundary condition was assigned to AB. The initial suction in fine-grained soil was selected to be 50 kPa, while that in coarse-grained soil was selected to be 10 kPa. To investigate the effects of the thickness of the fine-grained layer, slope angle, and rainfall intensity on the determination of the diversion length, the thicknesses of the fine-grained layer was considered to be 0.3, 0.5, 0.7, and 1.0 m, while rainfall intensities in the seepage analyses were considered to be 0.01, 0.1, 0.5, and 1.0 k_s of fine-grained soils, respectively. The slope angles ranged from 20° to 70° at 10° intervals.

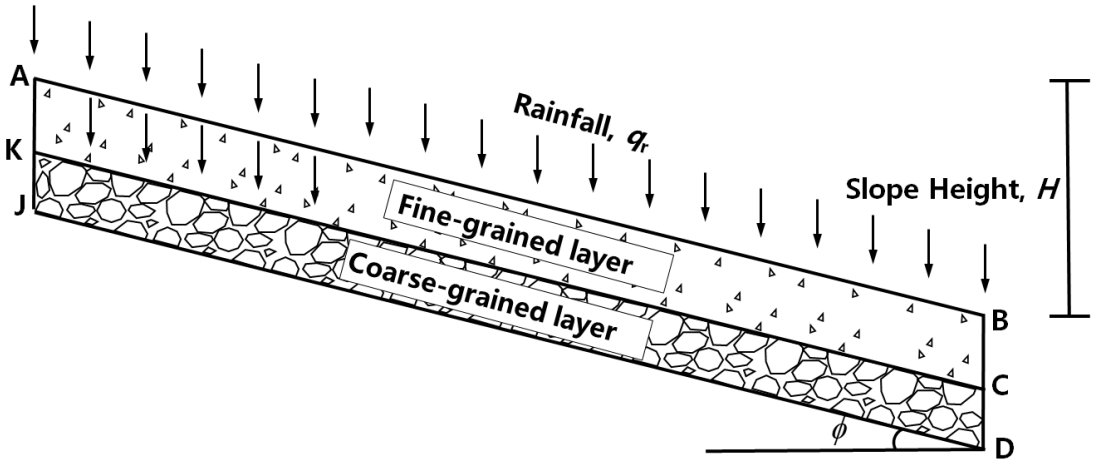

Figure 5. Illustration of the geometry and boundary conditions for the seepage analysis.

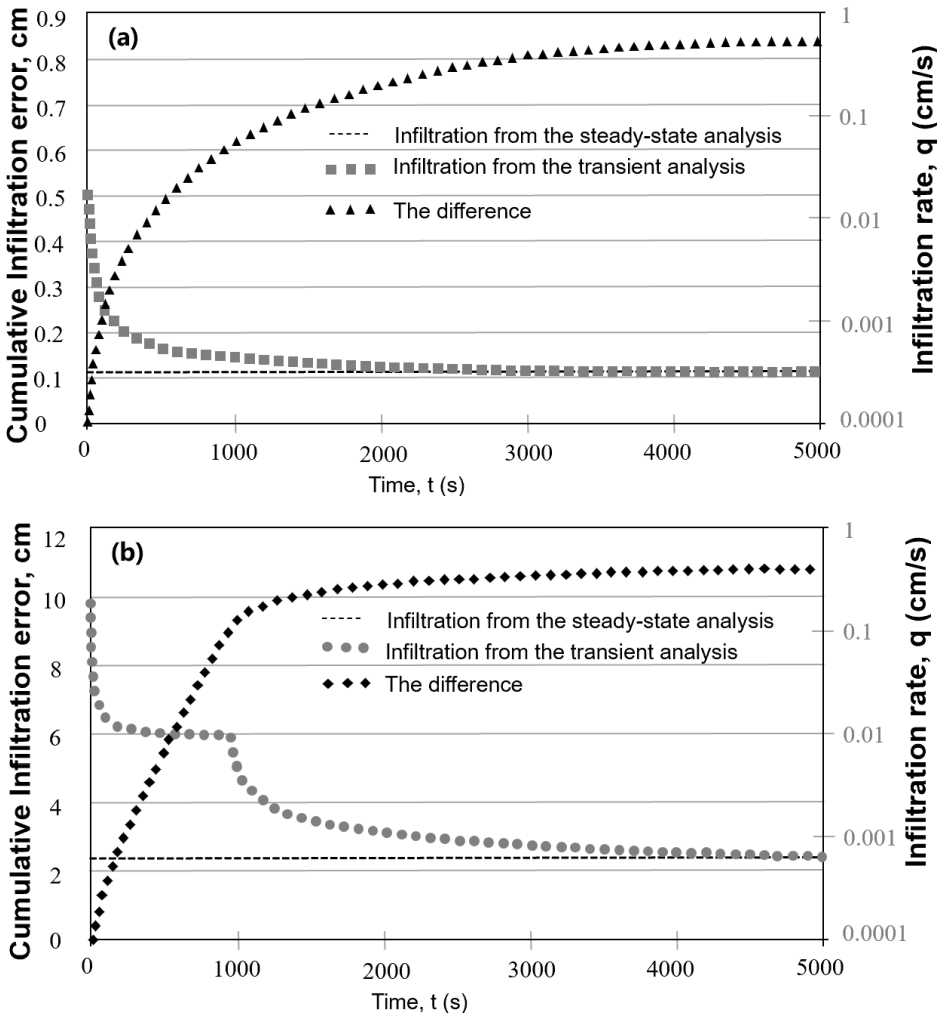

Figure 6. Infiltration results from both steady-state and transient analyses (modified from Blasch et al. [31]): (a) silt overlying sand and (b) sand overlying silt.

The total waterhead was determined using Darcy's law, where two-dimensional transient infiltration could be expressed as follows:

$$\frac{\partial}{\partial x}\left(k_x \frac{\partial H}{\partial x}\right)+\frac{\partial}{\partial y}\left(k_y \frac{\partial H}{\partial y}\right)+Q=\frac{\partial \theta}{\partial t} \tag{7}$$

where H is the total head, k_x is the hydraulic conductivity in the x-direction, k_y is the hydraulic conductivity in the y-direction, Q is the applied boundary flux, θ is the volumetric water content, and t is time.

As illustrated in Equations (2) and (7), in the steady-state infiltration analysis, the variation of water content with time is not considered, but the variation of water content is considered in the transient infiltration analysis. Blasch et al. [31] illustrated the different infiltration results from both steady-state and transient analyses, as shown in Figure 6.

As illustrated in Figure 6, the computed suction profile could be much different in the transient analysis than that from the steady-state analysis. On the other hand, Zhai et al. [32] provided definitions of SWCC variables, as shown in Figure 7. Those SWCC variables were adopted in this paper.

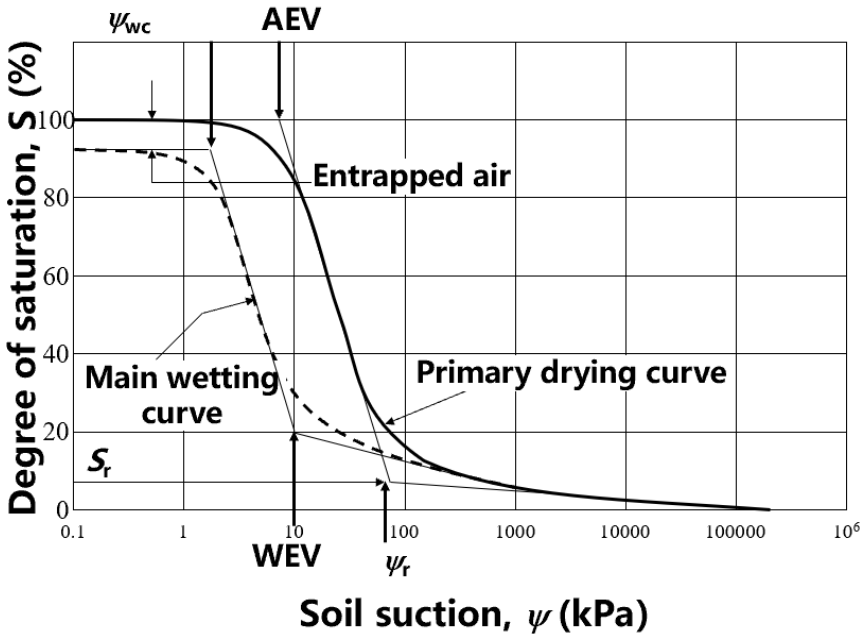

Figure 7. Illustration of the SWCC variables of both drying and wetting SWCCs (from Zhai et al. [32]).

Fredlund and Xing's equation [33], as shown in Equation (8), was adopted to represent the drying SWCC, while Zhai et al.'s equation [22], shown in Equation (9), was adopted to estimate the wetting SWCC from the drying SWCC. Subsequently, Zhai et al.'s method [23] was used to estimate the wetting HCF for those soils.

$$S = \left[1 - \frac{\ln\left(1+\frac{\psi}{C_r}\right)}{\ln\left(1+\frac{10^6}{C_r}\right)}\right] \frac{1}{\left\{\ln\left[e+\left(\frac{\psi}{a_f}\right)^{n_f}\right]\right\}^{m_f}} \tag{8}$$

where a_f, n_f, and m_f are the SWCC fitting parameters, and C_r is the input value.

$$S_{wet} = S(\psi_m) + \frac{S_0 - S(\psi_m)}{1 - S(\psi_m)} S(\psi)\left[S(k\psi) - S(\psi_m)\right] \tag{9}$$

where ψ_m is the initial suction in the wetting process, S_0 is the degree of saturation after the wetting process, and k is the parameter defining the contact angle difference in the drying and wetting processes. Zhai et al. [9] indicated that the fitting parameters in Fredlund and Xing's equation [33] with the form of volumetric water content are the same as those with the form of degree of saturation if the soil volume change could be ignored. In this paper, the soil volume change was assumed to be insignificant, and Fredlund and Xing's equation [33] with the form of degree of saturation was adopted.

The drying and wetting SWCCs for the fine- and coarse-grained soils, based on Rahardjo et al. [34], are illustrated in Figure 8(a). The saturated hydraulic conductivities for the fine- and coarse-grained soils were assumed to be 1×10^{-5} m/s and 3×10^{-3} m/s, respectively. Those SWCCs were adopted to estimate the wetting HCFs by using Zhai et al.'s method [23] for those soils, as illustrated in Figure 8(b). The SWCC parameters and saturated hydraulic conductivities are given in Table 1.

Table 1. SWCC parameters and saturated hydraulic conductivities of soils.

Soil	SWCC parameters						
	a_f	n_f	m_f	AEV	k	WEV	ψ_{wc}
Fine-grained soil	20	2	2	64.18	1.3	40	5.48
Coarse-grained soil	0.1	5	1	0.25	1.1	0.2	0.074

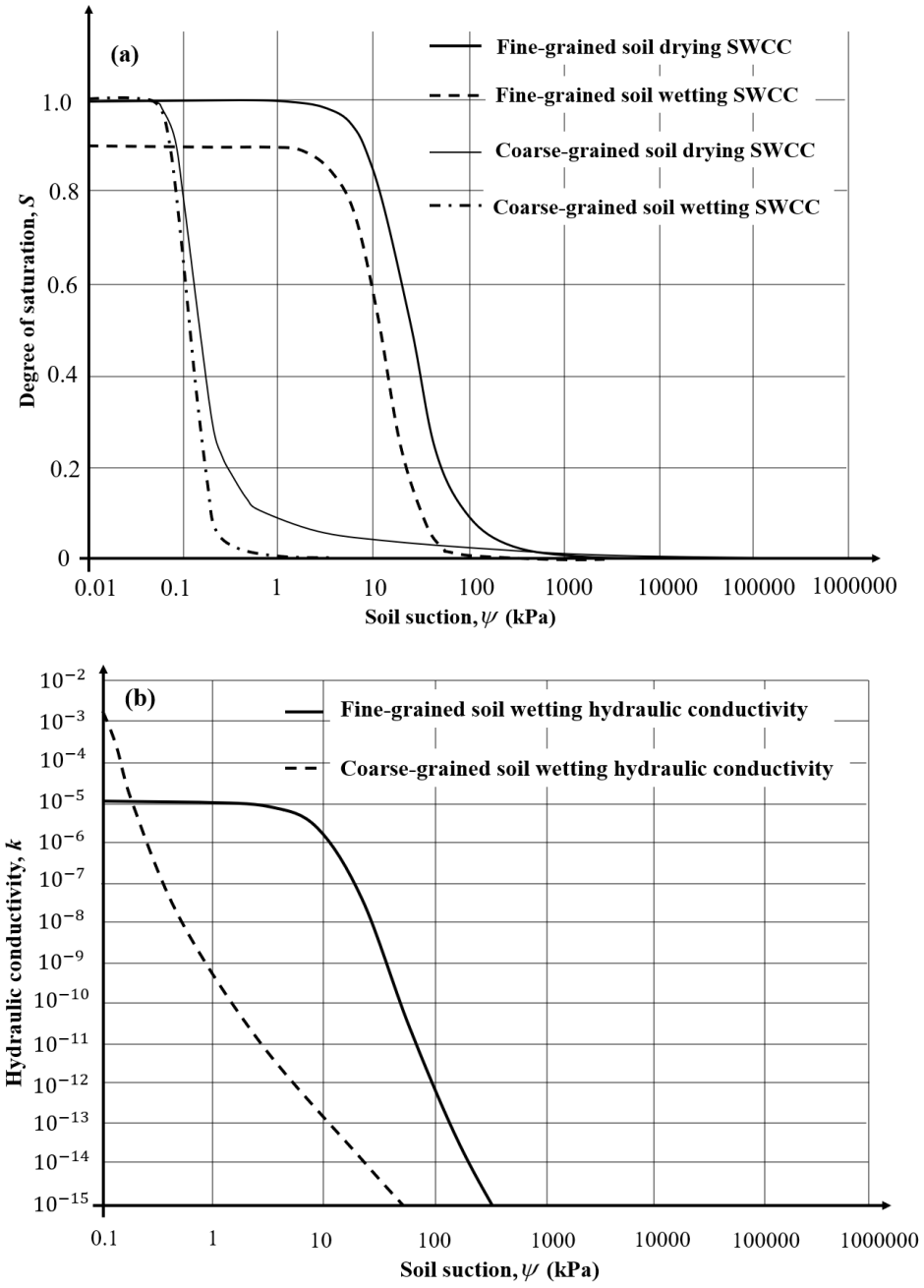

Figure 8. SWCCs and wetting hydraulic conductivities of soils for the seepage analysis. (a) SWCCs for the soils. (b) Wetting hydraulic conductivities for the soils.

The breakthrough condition was considered when the zero pore–water pressure in the coarse-grained layer was observed, as shown in Figure 9. The horizontal distance between the initial point and the breakthrough point was then defined as the diversion length.

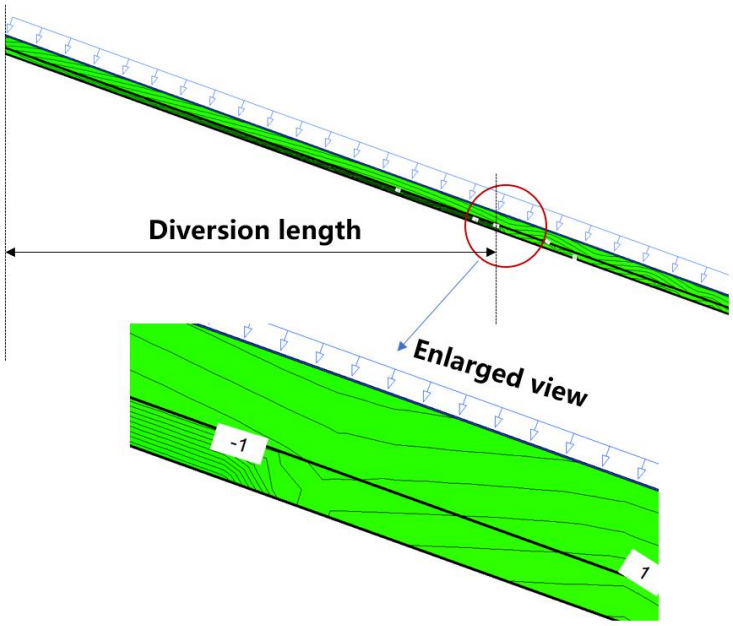

Figure 9. Criteria for the determination of the breakthrough condition from the result of seepage analysis.

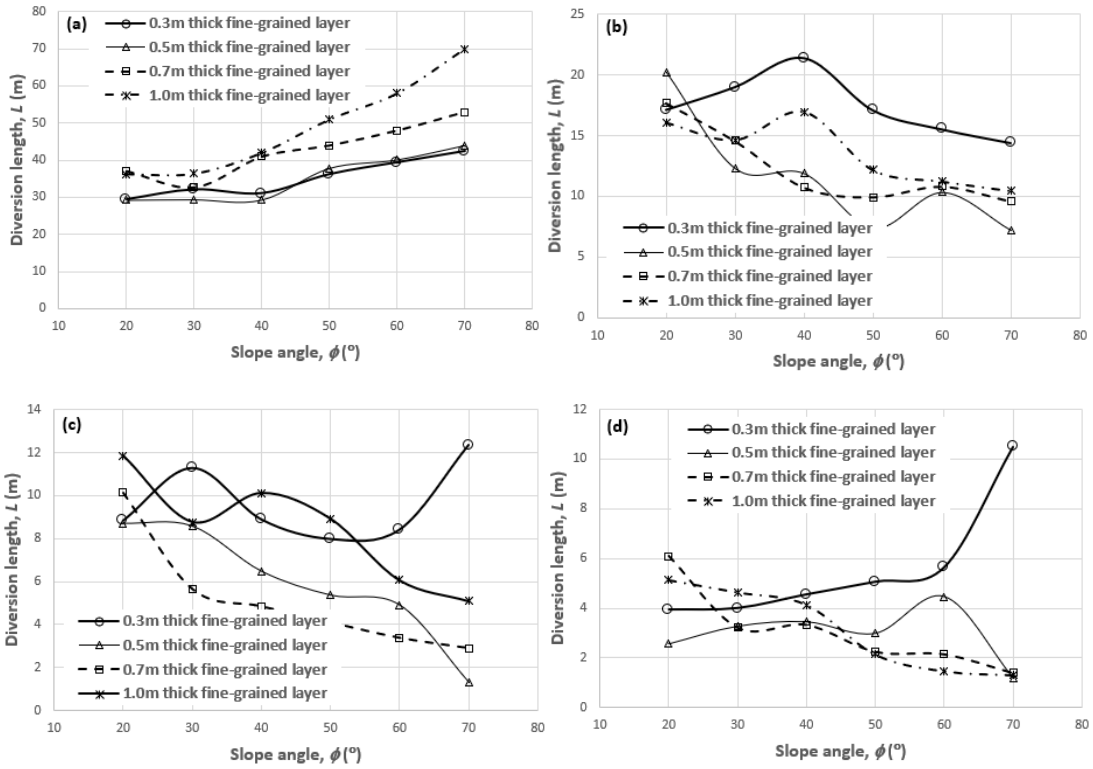

Figure 10. Diversion lengths from the numerical models. (a) Rainfall intensity equal to $0.01k_s$. (b) Rainfall intensity equal to $0.1k_s$. (c) Rainfall intensity equal to $0.5k_s$. (d) Rainfall intensity equal to k_s.

Based on the definition of the breakthrough, the diversion lengths and the times corresponding to the breakthrough condition were recorded for different cases and are illustrated in Table 2. The L_s obtained from the numerical analyses under different rainfall conditions and different thicknesses of the fine-grained layer are illustrated in Figure 10. On the other hand, the times corresponding to the breakthrough conditions for different cases are illustrated in Figure 11.

Table 2. Diversion length and corresponding time from numerical analyses.

Case	Th_f	f	q	t	L	Case	Th_f	f	q	t	L
1	0.3	20	$0.01k_s$	30.7	29.38	25	0.5	20	$0.01k_s$	51	29.21
2	0.3	30	$0.01k_s$	30.9	32.04	26	0.5	30	$0.01k_s$	53.3	29.34
3	0.3	40	$0.01k_s$	32.1	31.02	27	0.5	40	$0.01k_s$	53.5	29.23
4	0.3	50	$0.01k_s$	30.9	36.17	28	0.5	50	$0.01k_s$	52.3	37.8
5	0.3	60	$0.01k_s$	31.3	39.37	29	0.5	60	$0.01k_s$	50.9	40.11
6	0.3	70	$0.01k_s$	36.4	42.43	30	0.5	70	$0.01k_s$	51.1	44
7	0.3	20	$0.1k_s$	3.1	17.14	31	0.5	20	$0.1k_s$	5.1	20.24
8	0.3	30	$0.1k_s$	3.2	19	32	0.5	30	$0.1k_s$	5.1	12.31
9	0.3	40	$0.1k_s$	3.2	21.37	33	0.5	40	$0.1k_s$	5.1	11.90
10	0.3	50	$0.1k_s$	3.2	17.1	34	0.5	50	$0.1k_s$	5.2	7.4
11	0.3	60	$0.1k_s$	3.2	15.54	35	0.5	60	$0.1k_s$	5.2	10.35
12	0.3	70	$0.1k_s$	3.8	14.42	36	0.5	70	$0.1k_s$	5.2	7.22
13	0.3	20	$0.5k_s$	0.7	8.85	37	0.5	20	$0.5k_s$	1.1	8.69
14	0.3	30	$0.5k_s$	0.8	11.27	38	0.5	30	$0.5k_s$	1.1	8.57
15	0.3	40	$0.5k_s$	0.8	8.9	39	0.5	40	$0.5k_s$	1.1	6.48
16	0.3	50	$0.5k_s$	0.7	8.0	40	0.5	50	$0.5k_s$	1.1	5.37
17	0.3	60	$0.5k_s$	0.8	8.43	41	0.5	60	$0.5k_s$	1.1	4.91
18	0.3	70	$0.5k_s$	1.2	12.33	42	0.5	70	$0.5k_s$	1.1	1.33
19	0.3	20	k_s	0.4	3.94	43	0.5	20	k_s	0.7	2.56
20	0.3	30	k_s	0.5	4.0	44	0.5	30	k_s	0.7	3.27
21	0.3	40	k_s	0.5	4.55	45	0.5	40	k_s	0.7	3.45
22	0.3	50	k_s	0.4	5.06	46	0.5	50	k_s	0.7	2.99
23	0.3	60	k_s	0.6	5.64	47	0.5	60	k_s	0.6	4.46
24	0.3	70	k_s	0.8	10.5	48	0.5	70	k_s	1.0	1.19
Case	Th_f	f	q	t	L	Case	Th_f	f	q	t	L
49	0.7	20	$0.01k_s$	68.9	37.13	73	1.0	20	$0.01k_s$	92.9	36.26
50	0.7	30	$0.01k_s$	71	32.74	74	1.0	30	$0.01k_s$	93	36.4
51	0.7	40	$0.01k_s$	71.1	41	75	1.0	40	$0.01k_s$	93.6	42
52	0.7	50	$0.01k_s$	71.2	44	76	1.0	50	$0.01k_s$	94.2	51
53	0.7	60	$0.01k_s$	71.4	48	77	1.0	60	$0.01k_s$	94.0	58
54	0.7	70	$0.01k_s$	72	53	78	1.0	70	$0.01k_s$	94.3	70
55	0.7	20	$0.1k_s$	7.0	17.7	79	1.0	20	$0.1k_s$	9.5	16.07
56	0.7	30	$0.1k_s$	6.9	14.57	80	1.0	30	$0.1k_s$	9.6	14.64
57	0.7	40	$0.1k_s$	7.2	10.73	81	1.0	40	$0.1k_s$	9.9	16.96
58	0.7	50	$0.1k_s$	7.2	9.93	82	1.0	50	$0.1k_s$	10	12.16
59	0.7	60	$0.1k_s$	7.2	10.81	83	1.0	60	$0.1k_s$	10	11.22

Continued on next page

Case	Th_f	f	q	t	L	Case	Th_f	f	q	t	L
60	0.7	70	$0.1k_s$	7.3	9.58	84	1.0	70	$0.1k_s$	10	10.44
61	0.7	20	$0.5k_s$	1.5	10.15	85	1.0	20	$0.5k_s$	2.1	11.84
62	0.7	30	$0.5k_s$	1.5	5.66	86	1.0	30	$0.5k_s$	2.1	8.77
63	0.7	40	$0.5k_s$	1.6	4.85	87	1.0	40	$0.5k_s$	2.1	10.11
64	0.7	50	$0.5k_s$	1.6	4.1	88	1.0	50	$0.5k_s$	2.1	8.92
65	0.7	60	$0.5k_s$	1.6	3.38	89	1.0	60	$0.5k_s$	2.0	6.07
66	0.7	70	$0.5k_s$	1.6	2.9	90	1.0	70	$0.5k_s$	2.1	5.1
67	0.7	20	ks	0.8	6.09	91	1.0	20	ks	1.1	5.13
68	0.7	30	ks	0.8	3.22	92	1.0	30	ks	1.2	4.64
69	0.7	40	ks	0.8	3.33	93	1.0	40	ks	1.1	4.14
70	0.7	50	ks	0.8	2.25	94	1.0	50	ks	1.1	2.14
71	0.7	60	ks	0.9	2.15	95	1.0	60	ks	1.2	1.47
72	0.7	70	ks	0.9	1.40	96	1.0	70	ks	1.2	1.31

Note: Th_f denotes the thickness of the fine-grained layer (m), ϕ denotes the slope angle (°), q denotes the rainfall intensity, t denotes the time corresponding to the breakthrough condition (day), and L denotes the diversion length (m).

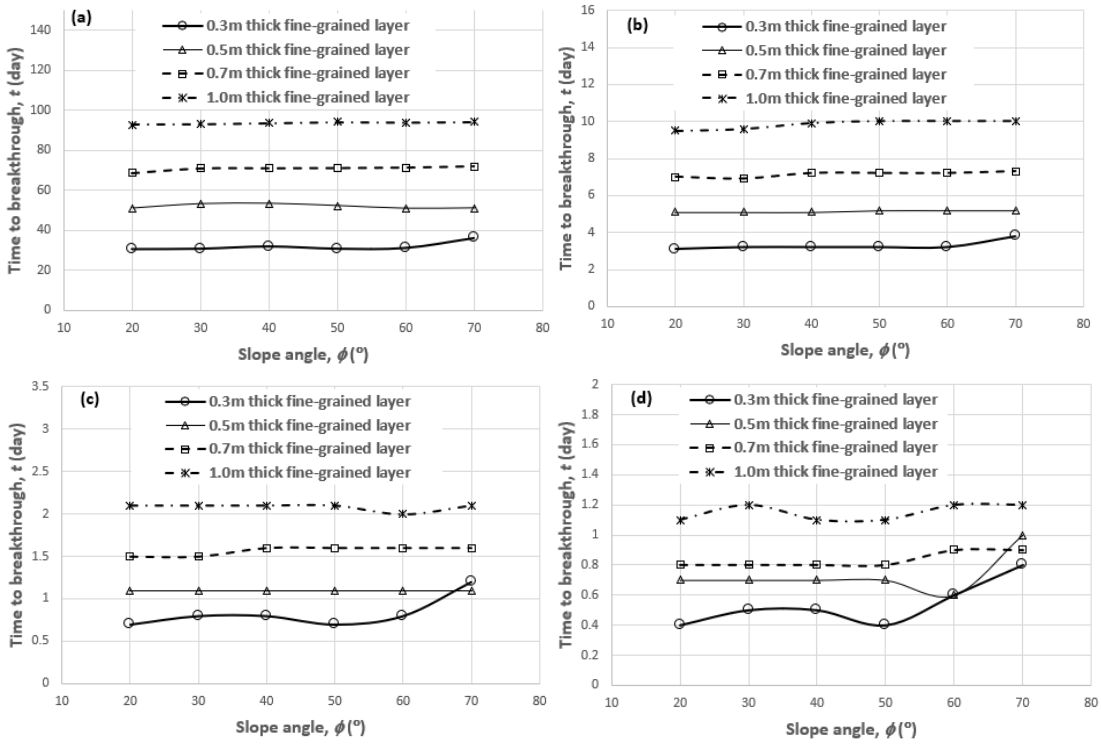

Figure 11. Illustration of the time corresponding to the breakthrough conditions from the numerical models. (a) Rainfall intensity equal to $0.01k_s$. (b) Rainfall intensity equal to $0.1k_s$. (c) Rainfall intensity equal to $0.5k_s$. (d) Rainfall intensity equal to k_s.

Figure 10 shows that when rainfall intensity was approximately 1% of k_s of the fine-grained soil, the diversion length increased with an increase in the slope angle, in agreement with the results from empirical equations. However, when the rainfall intensity was more than 10% of k_s of fine-grained

soil, the diversion length decreased with an increase in slope angle, which opposed the results from empirical equations. Figure 11 shows that the time corresponding to the breakthrough condition was a function of the thickness of the fine-grained layer and did not depend on the slope angle.

It is observed that Parent and Cabral's method [25] was an improvement of Ross [12] and Steenhuis et al.'s model [24]. On the other hand, Kung's method [21] was based on the theory of the funnel mechanism, which differed from the previous three models. Therefore, only the results from Kung [21] and Parent and Cabral's method [25] were computed and compared with the results from numerical analyses, as illustrated in Figure 12. Figure 12 indicates that when rainfall intensity was less than 10% of k_s of fine-grained soil, the results from Kung [21] and Parent and Cabral's method [25] would overestimate L of CBS. When rainfall intensity was higher than 50% of k_s of fine-grained soil, the results from Kung [21] and Parent and Cabral's method [25] would underestimate L of CBS. Figure 12 also indicates that the results from Kung's method [21] were closer to the numerical results than those from Parent and Cabral's method [25].

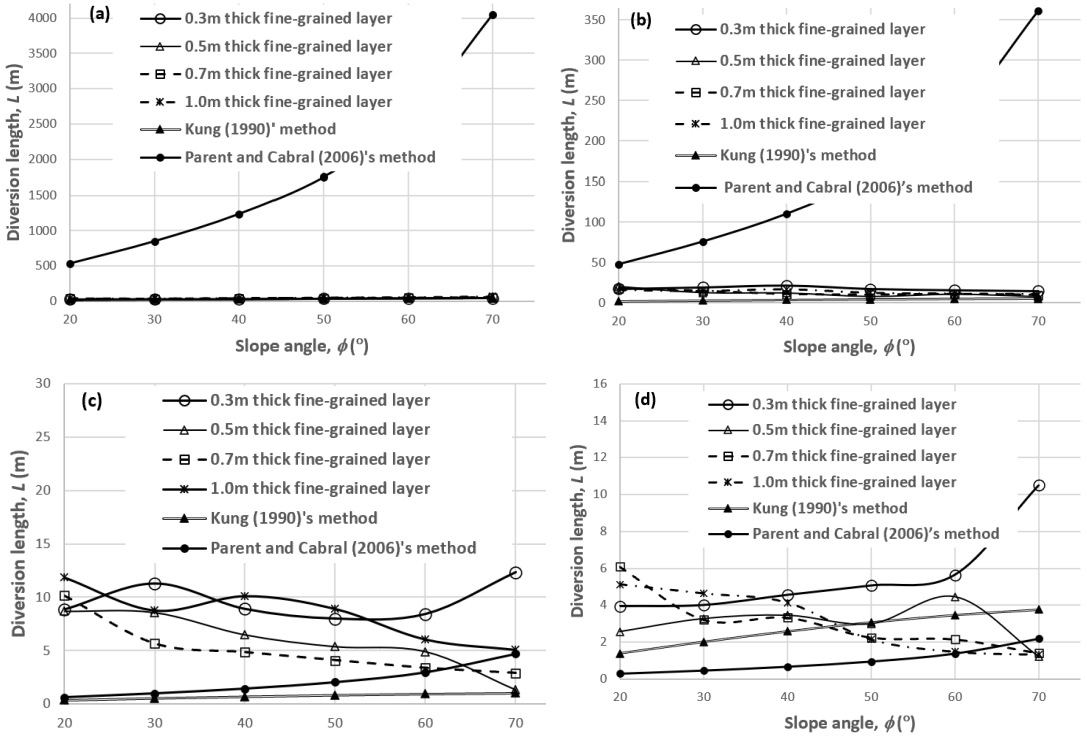

Figure 12. Illustration of the determined L using Kung [21] and Parent and Cabral's methods [25] and the numerical analyses. (a) Rainfall intensity equal to $0.01k_s$. (b) Rainfall intensity equal to $0.1k_s$. (c) Rainfall intensity equal to $0.5k_s$. (d) Rainfall intensity equal to k_s.

Figure 12 indicates that when rainfall intensity was less than $0.1k_s$ of fine-grained soil, the results from the empirical methods overestimate the diversion length. This means that the breakthrough may occur prior to the steady-state condition if the rainfall intensity is much higher than the k_s of fine-grained soil. On the other hand, with an increase in rainfall intensity (i.e., greater than $0.5k_s$), the results from the empirical methods may underestimate the diversion length, because most rainfall may become runoff and may not fully infiltrate into the soil.

4. Conclusions

The empirical models for the determination of the diversion length of CBS were reviewed, and the limitations associated with those models were explained. In the empirical models, the steady-state infiltration analysis was adopted, and it might not be applicable to the unsaturated soil. The diversion length of CBS should be analyzed by using transient infiltration analysis. It was observed that when the rainfall intensity was much lower than the k_s of fine-grained soil (e.g., less than 10%), the empirical model would overestimate L of CBS. On the other hand, when the rainfall intensity was higher than 50% of the k_s of fine-grained soil, the empirical model would underestimate the L of CBS. The numerical results indicated that when rainfall intensity was higher than 10% of the k_s of fine-grained soil, L decreased with an increase in the slope angle. The numerical results also indicated that the time to breakthrough was dependent on the thickness of the fine-grained layer, regardless of the slope angle.

Author contributions

Shijun Wang, Xianting Yi: Conceptualization, Methodology, Software, Validation; Yunfei Tian, Jing Yang, Huihui Xu, Hailong Zhang: Data curation, Formal analysis，Software; Qian Zhai: Conceptualization, Methodology, Supervision, Resources.

Use of AI tools declaration

The authors declare they have not used Artificial Intelligence (AI) tools in the creation of this article.

Acknowledgments

We would like to thank Enterprise Development Grant (Co-Innovation Program): BZ2023016 (Jiangsu) and CIP-2207-CN1064 (Singapore), Fujian Provincial Department of Transportation Science and Technology Development Project (JC202321).

Conflict of interest

The authors declare that they have no known competing financial interests or personal relationships that could have appeared to influence the work reported in this paper.

References

1. Fourie A (1996) Predicting rainfall-induced slope instability. *Proc Inst Civil Eng Geotech Eng* 119: 211–218. https://doi.org/10.1680/IGENG.1998.30117
2. Rahardjo H, Ong TH, Rezaur RB, et al. (2007) Factors controlling instability of homogeneous soil slopes under rainfall. *J Geotech Geoenviron Eng* 133: 1532–1543. https://doi.org/10.1061/(ASCE)1090-0241(2007)133:12(1532)

3. Rahardjo H, Kim Y, Gofar N, et al. (2020) Analyses and design of steep slope with GeoBarrier system (GBS) under heavy rainfall. *Geotext Geomembranes* 48: 157–169. https://doi.org/10.1016/j.geotexmem.2019.11.010
4. Zhai Q, Tian G, Ye WM, et al. (2022) Evaluation of unsaturated soil slope stability by incorporating soil-water characteristic curve. *Geomech Eng* 28: 637–644. https://doi.org/10.12989/gae.2022.28.6.637
5. Zhang LL, Zhang J, Zhang LM, et al. (2011) Stability analysis of rainfall-induced slope failure: a review. *Proc Inst Civil Eng Geotech Eng* 164: 299–316. https://doi.org/10.1680/geng.2011.164.5.299
6. Nicholson RV, Gillham RW, Cherry JA, et al. (1989) Reduction of acid generation in mine tailings through the use of moisture-retaining cover layers as oxygen barriers. *Can Geotech J* 26: 1–8. https://doi.org/10.1139/t89-001
7. Stormont JC, Morris CE (1998) Method to estimate water storage capacity of capillary barriers. *J Geotech Geoenviron* 124: 297–302. https://doi.org/10.1061/(ASCE)1090-0241(1998)124:4(297)
8. Rahardjo H, Santoso VA, Leong EC, et al. (2012) Performance of an Instrumented Slope Covered by a Capillary Barrier System. *J Geotech Geoenviron Eng* 138: 481–490. https://doi.org/10.1061/(ASCE)GT.1943-5606.0000600
9. Zhai Q, Rahardjo H, Satyanaga A (2017) Effects of residual suction and residual water content on the estimation of permeability function. *Geoderma* 303: 165-177. https://doi.org/10.1016/j.geoderma.2017.05.019
10. Zhai Q, Rahardjo H, Satyanaga A, et al. (2017) Effect of bimodal soil-water characteristic curve on the estimation of permeability function. *Eng Geol* 230: 142–151. https://doi.org/10.1016/j.enggeo.2017.09.025
11. Zhai Q, Rahardjo H, Satyanaga A (2019) Estimation of air permeability function from soil-water characteristic curve. *Can Geotech J* 56: 505–513. https://doi.org/10.1139/cgj-2017-0579
12. Ross B (1990) The diversion capacity of capillary barriers. *Water Resour Res* 26: 2625–2629. https://doi.org/10.1029/WR026i010p02625
13. Stormont JC (1996) The effectiveness of two capillary barriers on a 10% slope. *Geotech Geol Eng* 14: 243–267. https://doi.org/10.1007/BF00421943
14. Ng CWW, Liu J, Chen R, et al. (2015) Physical and numerical modeling of an inclined three-layer (silt/gravelly sand/clay) capillary barrier cover system under extreme rainfall. *Waste Management* 38: 210–221. https://doi.org/10.1016/j.wasman.2014.12.013
15. Chen R, Liu J, Ng CWW, et al. (2019) Influence of Slope Angle on Water Flow in a Three-Layer Capillary Barrier Soil Cover under Heavy Rainfall. *Soil Sci Soc Am J* 83: 1637–1647. https://doi.org/10.2136/sssaj2019.05.0135
16. Hill DE, Parlange JY (1972) Wetting Front Instability in Layered Soils. *Soil Sci Soc Am Pro* 36: 697–702. https://doi.org/10.2136/sssaj1972.03615995003600050010x
17. Stormont JC, Anderson CE (1999) Capillary barrier effect from underlying coarser soil layer. *J Geotech Geoenviron* 125: 641–648. https://doi.org/10.1061/(ASCE)1090-0241(1999)125:8(641)
18. Shackelford CD, Chang CK, Chiu TF (1994) The capillary barrier effect in unsaturated flow through soil barriers. ICEG TPCos, 1st International congress on environmental geotechnics. Edmonton, Canada: Thomas Telford, 789–793.
19. Stormont JC (1995) The effect of constant anisotropy on capillary barrier performance. *Water Resour Res* 31: 783–785. https://doi.org/10.1029/94WR03001

20. Yang H, Rahardjo H, Leong EC, et al. (2004) A study of infiltration on three sand capillary barriers. *Can Geotech J* 41: 629–643. https://doi.org/10.1139/t04-021
21. Kung KJS (1990) Preferential flow in a sandy vadose zone: 2. Mechanism and implications. *Geoderma* 46: 59–71. https://doi.org/10.1016/0016-7061(90)90007-V
22. Zhai Q, Rahardjo H, Satyanaga A, et al. (2020) Estimation of the wetting scanning curves for sandy soils. *Eng Geol* 272: 8. https://doi.org/10.1016/j.enggeo.2020.105635
23. Zhai Q, Rahardjo H, Satyanaga A, et al. (2021) Estimation of wetting hydraulic conductivity function for unsaturated sandy soil. *Eng Geol* 285. https://doi.org/10.1016/j.enggeo.2021.106034
24. Steenhuis TS, Parlange J, Kung KJS (1991) Comment on "The Diversion Capacity of Capillary Barriers" by Benjamin Ross. *Water Resour Res* 27: 2155–2156. https://doi.org/10.1029/91WR01366
25. Parent SÉ, Cabral A (2006) Design of Inclined Covers with Capillary Barrier Effect. *Geotech Geol Eng* 24: 689–710. https://doi.org/10.1007/s10706-005-3229-9
26. Liu J, Chen R, Ng CWW (2015) Discussion of "Physical and numerical study of lateral diversion by three-layer inclined capillary barrier covers under humid climatic conditions". *Can Geotech J* 52: 530–531. https://doi.org/ 10.1139/cgj-2014-0548
27. Rahimi A, Rahardjo H, Leong EC (2010) Effect of hydraulic properties of soil on rainfall-induced slope failure. *Eng Geol* 114: 135–143. https://doi.org/10.1016/j.enggeo.2010.04.010
28. Liu JX, Liu YT, Hu QJ (2010) Stability of embankment slope subjected to rainfall infiltration considering both runoff-underground seepage and fluid-solid coupling. *Rock Soil Mech* 31: 903–910.
29. Cuomo S, Della SM (2013) Rainfall-induced infiltration, runoff and failure in steep unsaturated shallow soil deposits. *Eng Geol* 162: 118–127. https://doi.org/10.1016/j.enggeo.2013.05.010
30. Liu Q, Su L, Zhang C, et al. (2022) Dynamic variations of interception loss-infiltration-runoff in three land-use types and their influence on slope stability: An example from the eastern margin of the Tibetan Plateau. *J Hydrol* 612: 128218. https://doi.org/10.1016/j.jhydrol.2022.128218
31. Blasch KW, Ferré TPA, Hoffmann JP, et al. (2006) Relative contributions of transient and steady state infiltration during ephemeral streamflow. *Water Resour Res* 42: W08405. https://doi.org/10.1029/2005WR004049
32. Zhai Q, Dai GL, Wang Hao, et al. (2024) Principles of unsaturated soil mechanics, China Architecture & Building Press.
33. Fredlund DG, Xing A (1994) Equations for the soil-water characteristic curve. *Can Geotech J* 31: 521–532. https://doi.org/10.1139/t94-061
34. Rahardjo H, Zhai Q, Satyanaga A, et al. (2015) Geo-Barrier System as a retaining structure, 6th Asia-Pacific *Conference on Unsaturated Soils. Guilin*, China, 871–876. https://doi.org/10.1201/b19248-146

AIMS Press